Microscopic studies on ALA-incubated tumor cells and tumor spheroids

Karsten König*,**, Herbert Schneckenburger**,*****, Heinrich Walt***,
Thomas Leemann****, Marie-Therese Wyss-Desserich*, Angelika Rück**,
and Bruce Tromberg*

*Beckman Laser Institute and Medical Clinic, Irvine, CA-92715
** Institute of Lasertechnology in Medicine, D-89081 Ulm
*** Dept. of Gynecology and Obsterics, Univ. Hospital, CH-8091 Zürich
**** Institute of Biomedical Engineering, Univ. and ETH, CH-8091 Zürich
***** Fachhochschule Aalen, Dept. of Optoelectronics, D-73430 Aalen

ABSTRACT

Various microscopy techniques were empoyed to measure subcellular porphyrin distribution in ALA-incubated tumor cells and tumor spheroids. In addition, photodynamically-induced intracellular changes in morphology and fluorescence were detected. Studies were carried out by confocal laser scanning microscopy, polarization microscopy, video-intensified microscopy, video-enhanced contrast microscopy, time-resolved and time-gated spectroscopy, and spectrally-resolved fluorescence imaging using a tunable liquid crystal filter. It was found, that ALA-incubation results in the biosynthesis of protoporphyrin IX (PP IX) in the mitochondria. Long ALA incubation times (>6 h) results in PP IX release to the cytoplasm. PP IX fluorescence has a maximum at 635 nm and a fluorescence decay time of 16 ns. No evidence for the existence of short-lived dimers, aggregates of PP IX, or other porphyrins was found. Cell irradiation resulted in cytotoxic reactions which, in turn, led to mitochondrial swelling followed by destruction of the cell membrane. In addition, PP IX photodestruction and the formation of short-lived chlorin-type photoproducts were observed.

1. INTRODUCTION

The external administration of the heme precursor 5-aminolevulinic acid (ALA) to tumor cells results in the intracellular formation of photosensitizing fluorescent porphyrins, which can be used for photodynamic therapy (PDT) of cancer and other diseases[1,2,3].

These porphyrins can be detected by fluorescence measurements. Spectral behaviour and fluorescence decay kinetics can provide information regarding porphyrin type, microenvironment, and degree of aggregation. For example, fluorescence maxima of zinc-protoporphyrin IX, coproporphyrin, and protoporphyrin IX (PP) in dimethylsulfoxide (DMSO) are 592 nm, 622 nm, and 635 nm, respectively.. In solvents of higher polarity, like water, the maxima are blue-shifted by 10 - 20 nm. Fluorescence-altering aggregation of metal-free porphyrins may occur in aqueous solution. Monomers have, in general, fluorescence decay times between 10 and 20 ns, dimers about 2 ns, and higher aggregates possess lifetimes in the ps-region[4,5,6]. Emission maxima of aggregates are red shifted compared to monomers. However, steady-state fluorescence spectra are dominated by their monomer emission due to the high fluorescence quantum yield.

The goal of this study was to investigate ALA-induced intracellular porphyrin formation and PDT-induced fluorescence modifications in single cells and spheroids using different microscopy techniques with high spatial, spectral, and temporal resolution.

2. MATERIALS AND METHODS

2.1. Video- and polarization microscopy

A high-resolution CCD camera (Horn, Aalen, Germany) and a highly sensitive SIT camera (Hamamatsu Photonics) were attached to the two external ports of a Zeiss fluorescence microscope. The microscope was equipped with polarizers, high-aperture DIC condensor, Wollaston prism, internal zoom (1-4x), and tension-free DIC objectives (63x 1.32, 100x 1.32). The light source for fluorescence exitation, Differential Interference Contrast (DIC) imaging, and photodynamically-induced cell damage was a 100 W high-pressure mercury lamp.

Video-Intensified Microscopy (VIM) for the detection of weakly fluorescent samples and Video-Enhanced Contrast Microscopy (VECM)[7] using DIC for visualization of subcellular structures were used. The contrast of the raw picture was improved by analogue- (adjusting camera gain and offset) and digital contrast enhancement (subtraction of out-of-focus background, averaging).

2.2. Confocal Laser Scanning Microscopy

Depth-resolved fluorescence studies were carried out with the Confocal Laser Scanning Microscope (CLSM) from Leica Instruments. Fluorescence excitation was provided by the 488 nm line of an argon ion laser. Fluorescence was detected in the range 580 nm - 800 nm. The thickness of the slices varied between 1 μm and 2.5 μm. The resulting stack of CLSM image slices with a resolution of 512 by 512 pixels each was processed by the modular software system QUASIA3D (QUantitative Analytical System for Image Acquisition in 3D). In order to quantify the spatial density distribution of the photosensitive agents in the cell population we used a multi-level, true 3D-processing scheme[8].

2.3. Spectrally-resolved fluorescence imaging

Spectrally-resolved fluorescence images of 407nm-excited cells were obtained with a slow-scan, cooled CCD camera (Princeton Instruments) combined with a birefringent liquid crystal filter (VariSpec, Cambridge Research and Instrumentation).

2.4. Fluorescence decay kinetics and time-gated microscopy

Time-gated images in the nanosecond region were obtained by fluorescence excitation with a frequency-doubled Q-switched Nd:YAG laser (532 nm, 2 ns, fiber-guided to the microscope) and a highly sensitive camera (Proxitronic, NCA) with gateable image intensifier (minimal time gate: 5 ns), as described previously[9-11]. Fluorescence decay kinetics were measured using a frequency-doubled laser diode (390 nm, Hamamatsu Photonics) and time-correlated single photon counting electronics[10].

2.5. Samples

Estrogen-dependent mammary carcinoma cells MCF-7 (ISREC, Lausanne), HEC-1-A cells (human endometrial adenocarcinoma cells in medium 199, Earle's Salts with 10% FCS, ATCC-nr. 112-HTB), CHO-K1 cells (Chinese hamster ovarian cells in MEM medium with 10% FCS, ATCC-nr.: CCL61), and RR 1022 epithelial cells (rat sarcoma, medium DMEM with 5% FCS) were used. MCF-7 spheroids with mean diameter of 0.15 mm were achieved by three-dimensional growth by cultivation on agar. ALA-incubated chorioalantoic membrane (CAM) of chicken embryos was used in time-resolved measurements. ALA (M= 168 g) was obtained from Sigma Products, diluted with NaOH, and buffered with PBS (pH= 7.1). Single cells and spheroids were incubated with 0.1 or 1 mg/ml ALA and 10 μg/ml Rhodamin 123.
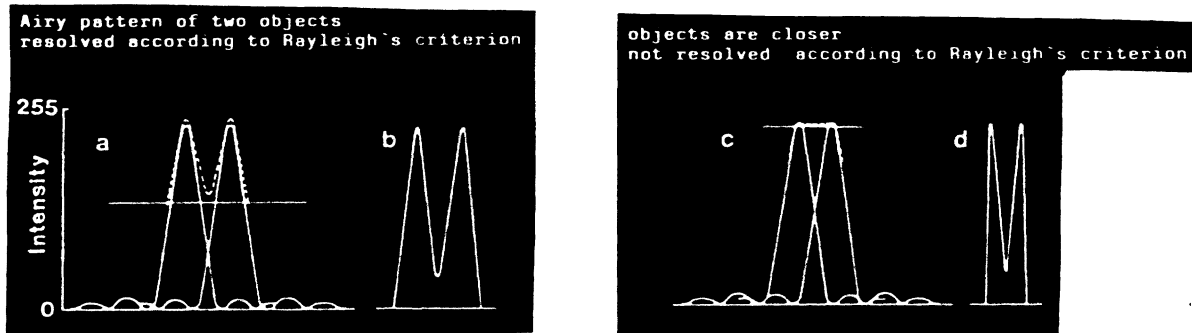
Fig. 1 Principle of Video-Enhanced Contrast Microscopy*. Resolution and contrast enhancement are achieved by increasing the threshold (offset) of the CCD camera and the magnification (gain) of the high-intensity part of the diffraction pattern.

3. RESULTS AND DISCUSSION

3.1. Video-Intensified Microscopy and Video-Enhanced Contrast Microscopy

Real-time fluorescence images in the detection range of 580 nm - 800 nm of ALA-incubated tumor epithelial cells during irradiation were obtained using VIM indicating the ALA-induced formation of intracellular fluorescence in the red. Fluorescence occurred within minutes of incubation and was detected for more than 24 hours in the case of unwashed cells. Rapid photobleaching occurred during light exposure with a bleaching factor (fluorescence intensity dropped to 37%) of about 5 J/cm^2 (400 nm - 440 nm, high pressure mercury lamp).

Fluorescence modifications correlated with changes in morphology. Visualization of PDT-induced subcellular damage in real time was achieved by VECM. This method enables the observation of intracellular organelles of living cells in the range of 100 nm[6], see Fig. 1. Figure 2 shows typical images of photodynamically-induced destruction of epithelial cells after ALA uptake. Light exposure resulted in significant changes in mitochondria morphology. In particular, a great part of these organelles lost their initial shape and rounded up. These intracellular changes were followed by damage to the cell membrane indicated by bubble formation and an increase in cell volume, Fig. 3.

3.2. Confocal Laser Scanning Microscopy

Fluorescence images performed on single mammary carcinoma cells (3 h ALA incubation) showed the efficient fluorophore biosynthesis in certain cell organelles. No emission occurred in the cell membrane and the nucleus. Fig. 4 exhibits an unprocessed, 1 μm fluorescence slice. Comparative measurements with the mitochondrial marker Rhodamin 123 results in nearly the same fluorescence pattern. Therefore, fluorophore biosynthesis and accumulation seems to occur in mitochondria.

Spheroids with an incubation time less than 6 hours exhibited a granular fluorescence pattern. Fluorescence was initially detected 10 min after ALA incubation indicating a high rate of porphyrin biosynthesis. When maintained in ALA-containing medium, the fluorescence pattern changed with time. A nearly homogenous emission pattern was found at 48 h, probably indicating the release of fluorescent porphyrins into cytoplasm, Fig. 5.
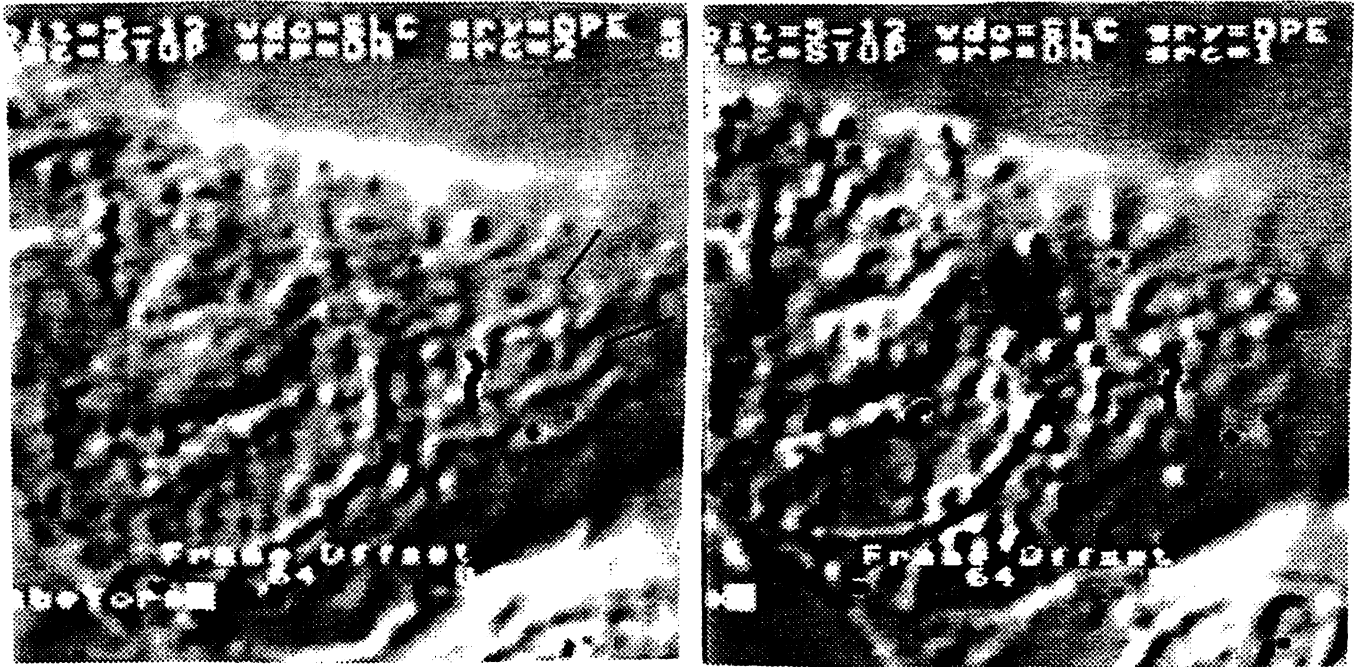
Fig. 2 VECM-images of ALA-incubated RR 1022 cells indicating photodynamically-induced mitochondria destruction (rounding up), right: before, left: after irradiation
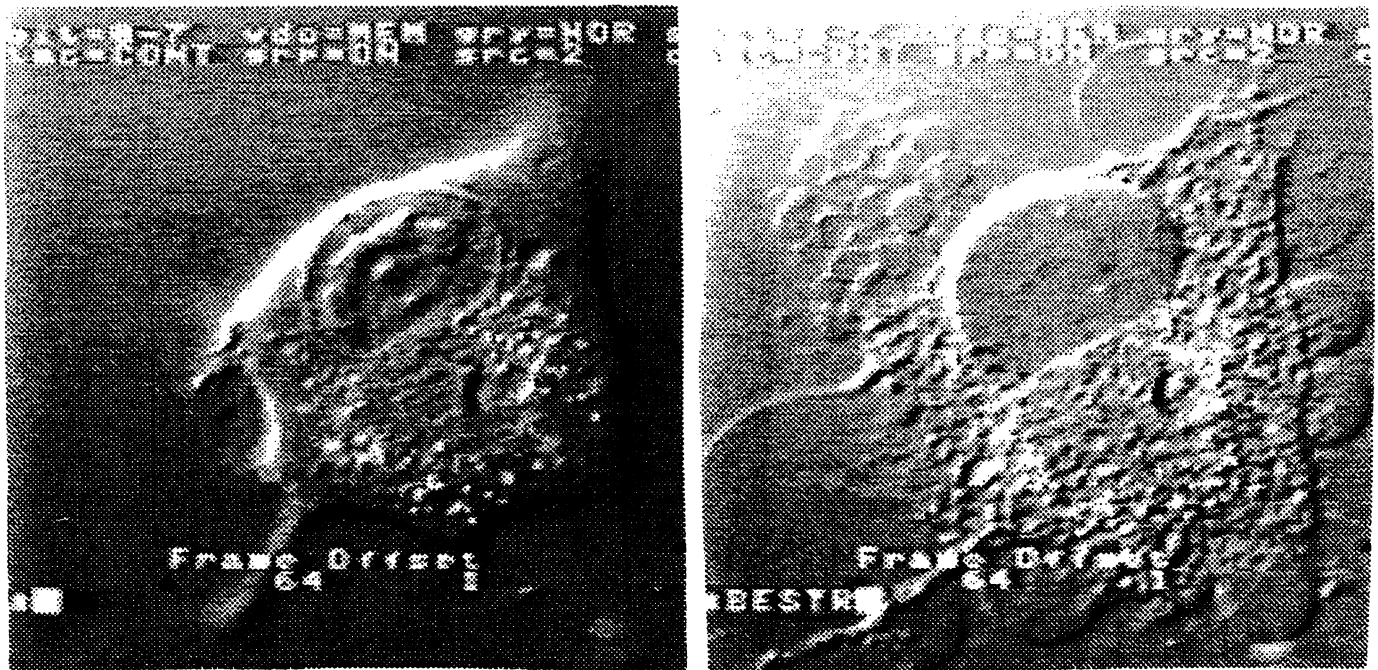
Fig. 3 After significant changes of mitochondrial morphology (left), damage of cell membrane (bubble formation) and blowing-up occur (right)
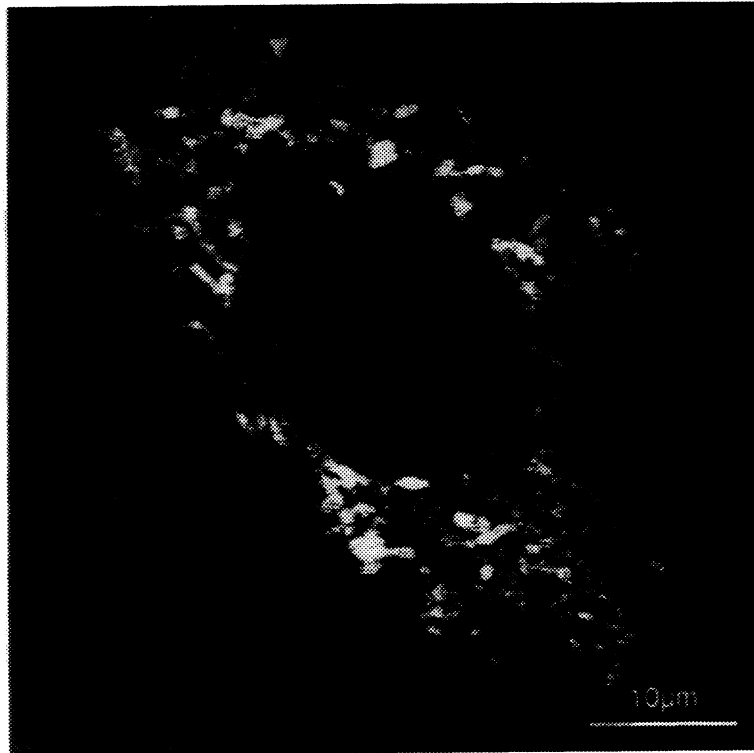
Fig. 4 CLSM fluorescence image (1 μm slice) of a single mamma carcinoma cell incubated with ALA for 3 hours
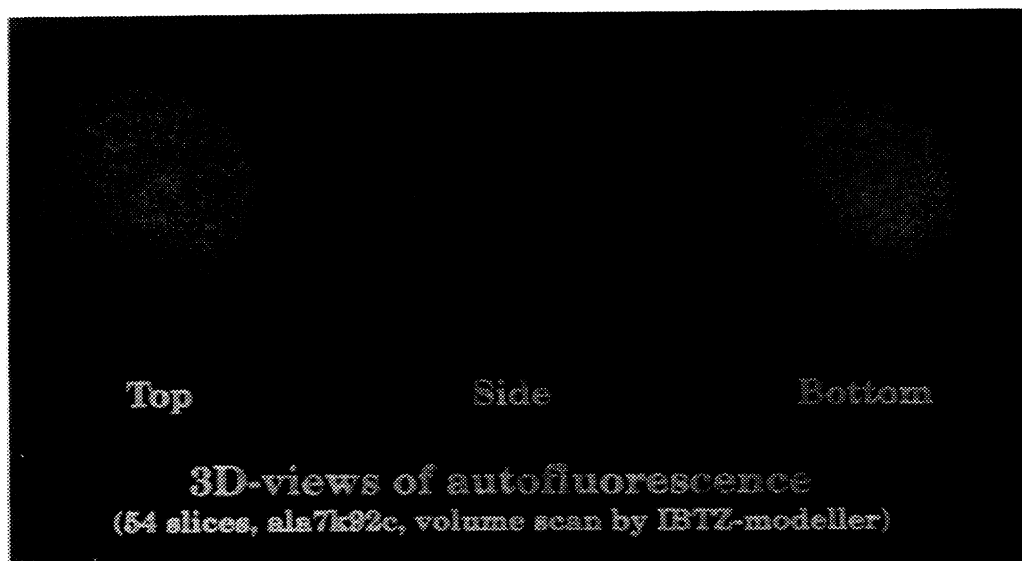

Fig. 5 Processed fluorescence images of an ALA-incubated spheroid

Irradiation of spheroids resulted in photodynamically-induced swelling and bubble formation. The efficiency of the irradiation was higher the longer the incubation time. For times longer than 4 hours, even fluorescence excitation radiation induced spheroid destruction, Fig. 6.
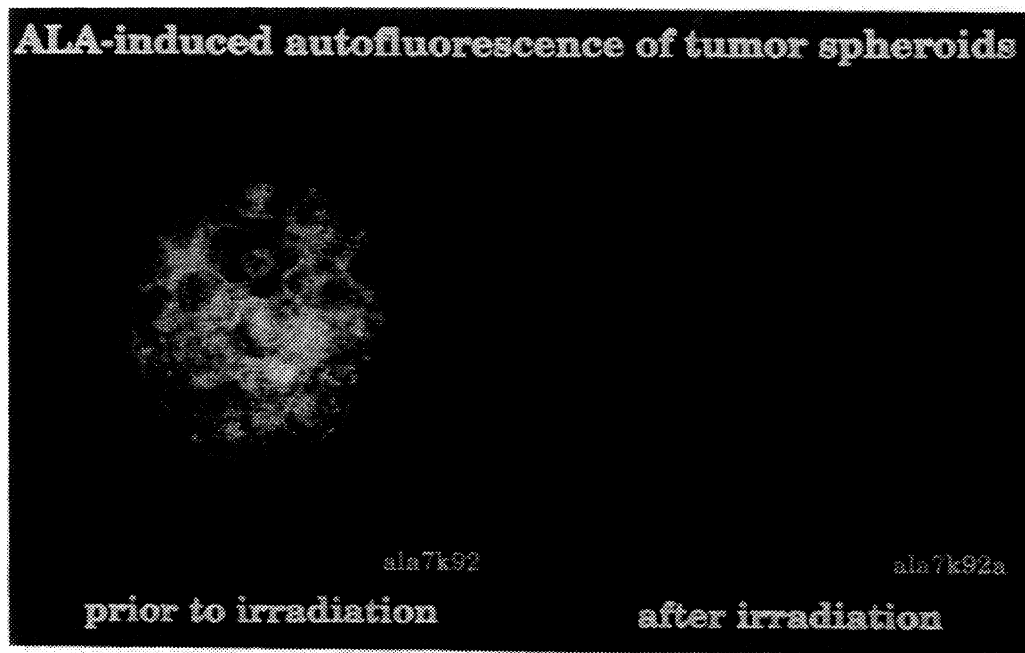

Fig. 6 Photodynamically-induced changes of the spheroid morphology

3.3. Spectrally-resolved cell imaging

Spectrally-resolved fluorescence images of ALA-incubated CHO cells are shown in Fig. 7. The long incubation time of 24 h resulted in cytoplasm and cell membrane fluorescence. Image analysis allowed the reconstruction of intracellular spectra indicating a pronounced emission between 630 and 640 nm. No significant differences between the spectra of various intracellular fluorescent spots were found. As shown in Fig. 8, the difference image of the images at 580 nm and 630 nm indicate variations in emission intensity only. There was no evidence for the presence of different red-emitting fluorophores.

3.4. Polarization microscopy

Fluorescence images with linearly polarized excitation light were acquired in order to detect fluorescent porphyrin aggregates. The emission of these high-molecular-weight, short-lived species with long rotational correlation times should possess a higher degree of fluorescence anisotropy than the monomer. No significant differences were found for ALA-incubated epithelial cells. In contrast, Photosan-incubated cells, showed for short incubation times (< 5 h), preferential accumulation of monomers in the cell membrane[12].
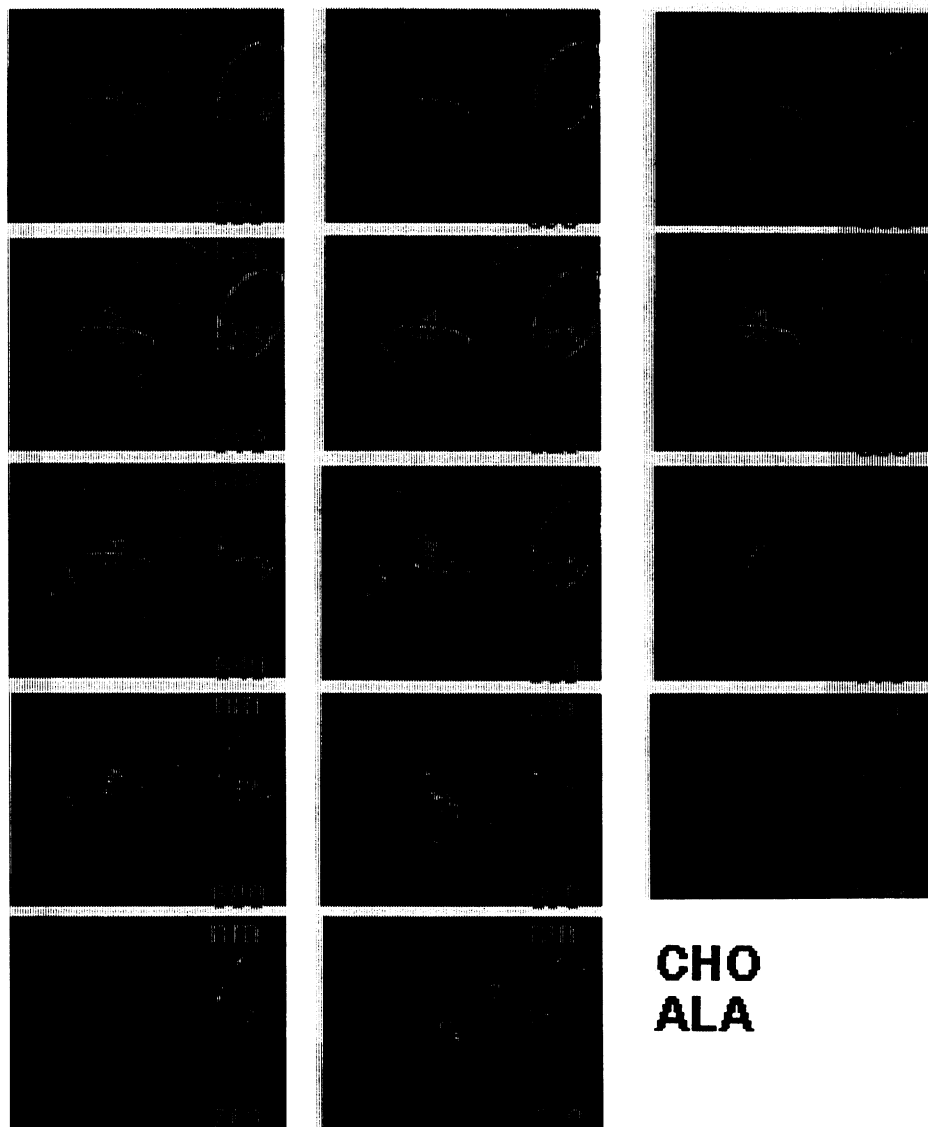
CHO
ALA

Fig. 7 Spectrally-resolved fluorescence images of CHO cells incubated with ALA for 24 hours. The intracellular fluorescence pattern of these long-incubated cells indicate porphyrin accumulation in cytoplasm and cell membrane. Maximal fluorescence intensity was achieved at 630 nm and 640 nm.
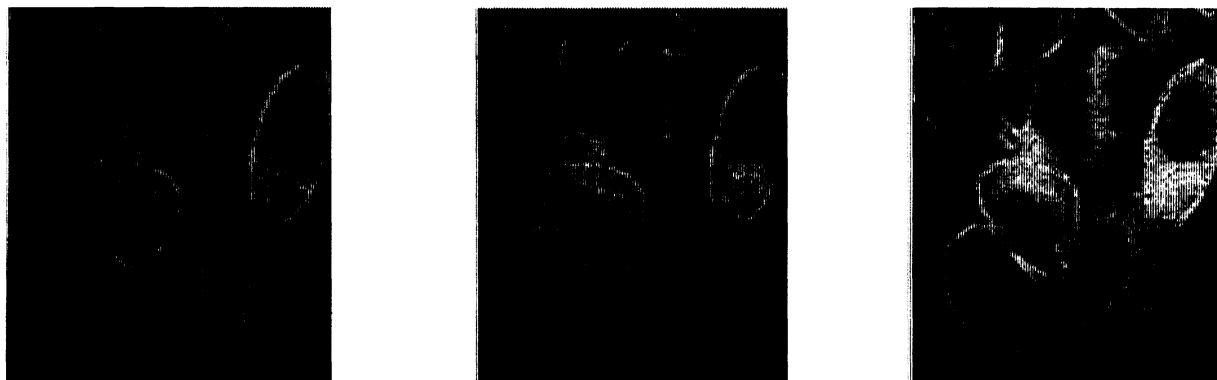
Fig. 8 Images of intracellular porphyrin fluorescence at 580 nm and 630 nm and difference image $(I_{630}-I_{580})$

3.5. Fluorescence decay kinetics and time-gated imaging

We measured time-integrated (cw) and time-gated images of single RR 1022 epithelial cells, incubated with ALA or Photosan for 3 hours. Significant differences between the cw image and the 5 ns time-gated image were observed for intracellular Photosan due to different accumulation sites of monomers, dimers, and higher aggregates. In particular, we detected localization of long-lived porphyrin monomers in the plasma membrane and short-lived components in the cytoplasm. In contrast, ALA-incubated cells showed no differences in intracellular, intensity-normalized, fluorescence pattern. Therefore, no evidence for short-lived fluorophores could be found for ALA-stimulated emission, Fig. 9.

The measurement of the fluorescence decay kinetics of ALA- and Photosan-incubated CAM supports the findings of polarization- and time-gated microscopy. Photosan decay kinetics are tri-exponential with decay times of about 13 ns, 2 ns and 0.2 ns. In contrast, ALA-incubated cells exhibit an almost monoexponential behavior with decay times of 16-18 ns, Fig. 10.

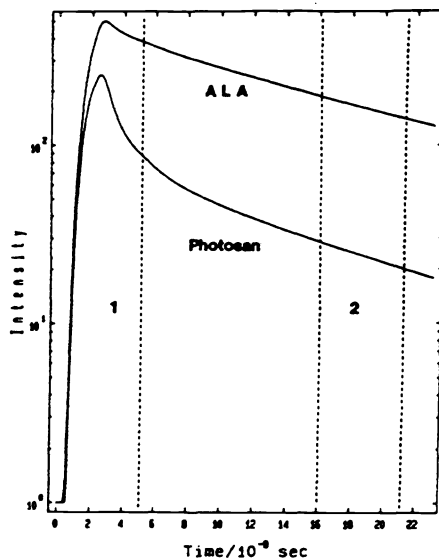It can therefore concluded, that the ALA-induced intracellular fluorophore is monomeric PP IX.

Fig. 10
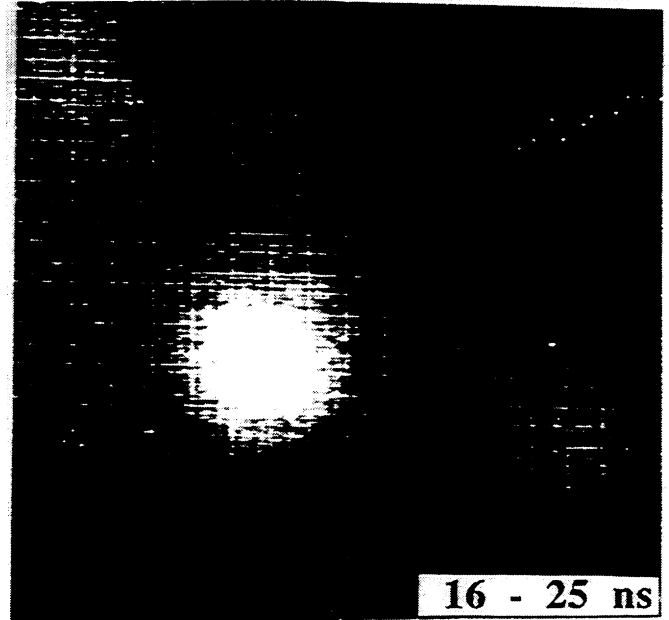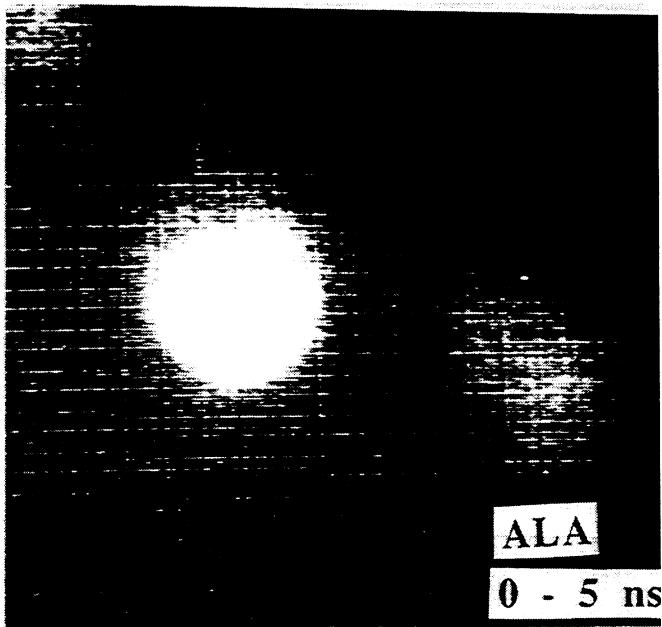Fluorescence decay kinetics of ALA-incubated CAM, which consists of about 3 cell layers
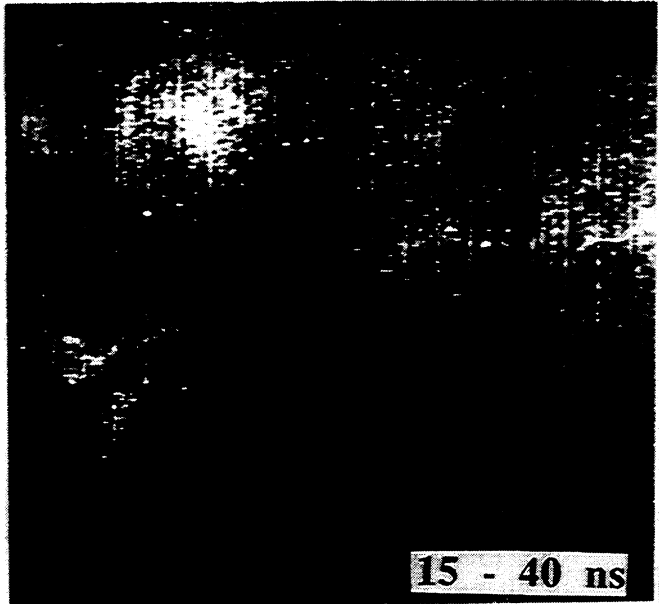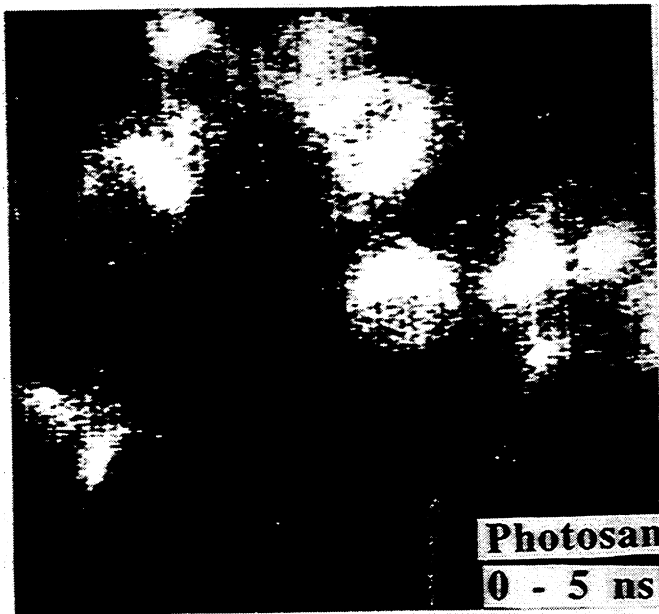
Fig. 9 Time-gated images of Photosan-incubated (upper part) and ALA-incubated RR 1022 cells (lower part)
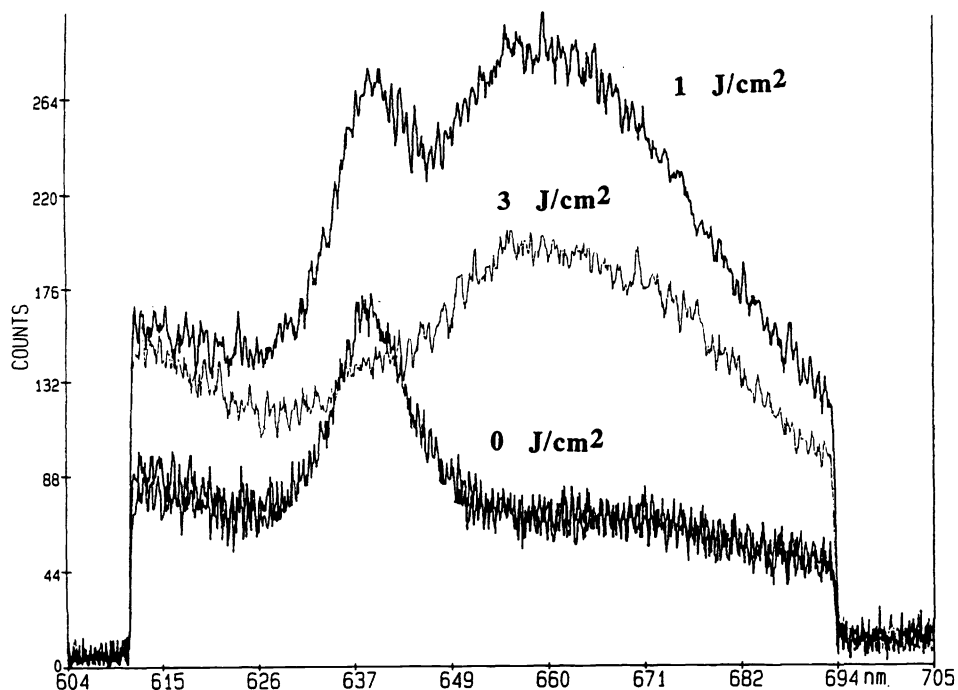
Fig. 11   Cell irradiation resulted in the formation of a new fluorescence band at 600 - 670 nm due to photoproduct formation
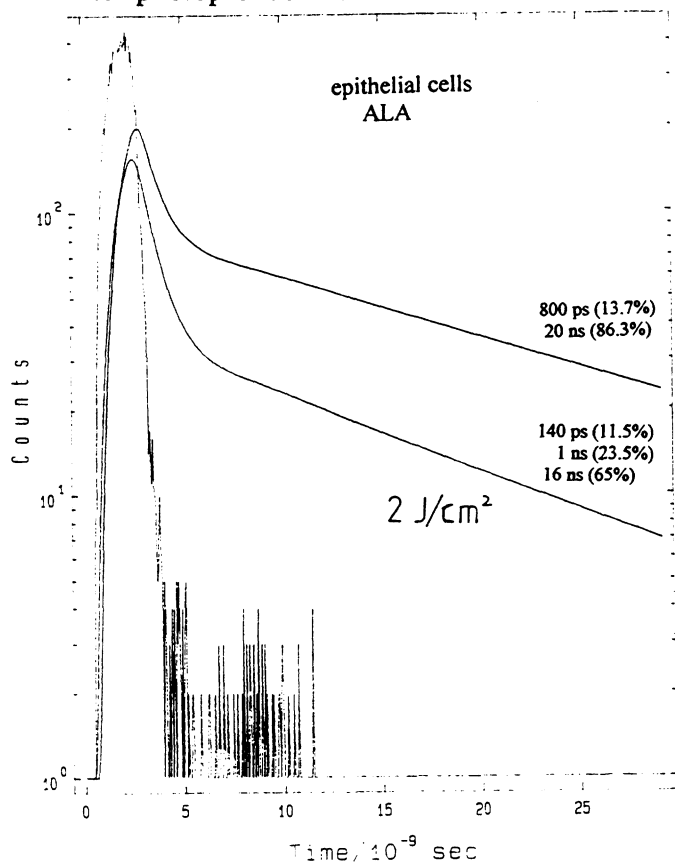

Fig. 12   Photoinduced shortening of the fluorescence decay kinetics. The short component of 800 ps in ALA-incubated epithelial cells can be explained by short-lived naturally-occurring fluorophores

3.6. Intracellular photodynamically-induced porphyrin-destruction

The photodestruction of ALA-induced intracellular PP IX was probed by spectroscopy on single cells. Light exposure to ALA-incubated cells resulted in cell death, and concomitant destruction of photosensitizer. Chlorin-type photoproducts emitting around 670 nm were formed inside the cell, as shown in Fig. 11. The formation of short-lived photoproducts led to a shortening of the fluorescence decay kinetics, Fig. 12. Recent studies revealed the singlet-oxygen dependence of these photochemical reactions[13].

4. REFERENCES

1. J.C. Kennedy and R.H. Pottier, "Endogenous protoporphyrin IX, clinically useful photosensitizer for photodynamic therapy", J. Photochem. Photobiol. B 14, pp. 275-292, 1992.

2. W.H. Boehncke, K. König, W. Scheffold, and W. Sterry, " Photodynamic therapy in psoriasis", Skin Pharmacol., in press.

3. K. König, H. Boehncke, A. Rück, R. Kaufmann, R. Steiner, and W. Sterry, "Photodynamic effects on T-cells and skin lesions of a patient with mycosis fungoides using porphyrin photosensitizers", Proceedings SPIE, Budapest, vol. 2086, 1993, in press.

4. M. Yamashita et al., "Picosecond time resolved fluorescence spectroscopy of HpD", IEEE-QE 20, pp. 1363-1369, 1984.

5. I. Bugiel, K. König, and H. Wabnitz, "Investigation of cells by fluorescence scanning microscopy with subnanosecond time resolution", Lasers Life Sci. 3, pp. 47-53, 1989.

6. K. König, H. Wabnitz, and W. Dietel, "Variation in the fluorescence decay properties of haematoporphyrin derivative during its conversion to photoproducts", J. Photochem. Photobiol. B 8, pp. 103-111, 1990.

7. D.G. Weiss, W. Maile, and R.A. Wick, "Video microscopy", in: A.J. Lacey (ed.), "Light Microscopy in Biology-A Practical Approach", IRL Press, Oxford, pp. 221-278.

8. T. Leemann, F. Margadant, H. Walt, B. Jentsch, U. Haller, and M. Anliker, "Computer Assisted 3D-Microscopy in Gynaecology: Photodynamic Therapy of Cancer Cells", ISPRS Comission V Intercongress Symposium, 1-4 March 94, Melbourne, Australia.

9. H. Schneckenburger, W. Strauss, A. Rück, H. Seidlitz, and J.M. Wessels, "Microscopic fluorescence spectroscopy and diagnosis", Opt. Eng. 31, pp. 995-999, 1992.

10. H. Schneckenburger, K. König, T. Dienersberger, and R. Hahn, "Time-gated microscopic imaging and spectroscopy in medical diagnosis and photobiology", Opt. Eng., in press.

11. H. Schneckenburger et al., "Time-resolved in-vivo fluorescence of photosensitizing porphyrins", J. Photochem. Photobiol. B 21, pp. 143-147, 1993.

12. H.K. Seidlitz, H. Schneckenburger, and K. Stettmeier, "Time-resolved polarization measurements of porphyrin fluorescence in solution and in single cells", J. Photochem. Photobiol. B 5, pp. 391-400, 1990.

13. K. König, H. Schneckenburger, A. Rück, and R. König, "Studies on Porphyrin Photoproducts in Solution, Cells, and Tumor Tissue", Proceedings, SPIE 1994, vol. 2133.